



## Potential existence of $\text{Xe}_3\text{CO}_2$ compounds with distinct Xe-C covalent bonds under pressures of Earth's core

Kang Yang,<sup>1,2</sup> Ke Yang,<sup>2</sup> Tong Yang,<sup>2</sup> Jingyu He ,<sup>2</sup> Ming Yang ,<sup>2,\*</sup> and Tong Zhou<sup>1,†</sup>

<sup>1</sup>*Eastern Institute for Advanced Study, Eastern Institute of Technology, Ningbo, Zhejiang 315200, China*

<sup>2</sup>*Department of Applied Physics, The Hong Kong Polytechnic University, HungHom, Hong Kong SAR, China*



(Received 10 February 2024; revised 14 June 2024; accepted 30 July 2024; published 19 August 2024)

Noble gas compounds have attracted significant research attention, mainly due to their intriguing chemical behavior under high-pressure conditions. In this paper, we identify a compound,  $C2/m\text{-Xe}_3\text{CO}_2$ , through a synergistic approach combining a particle-swarm optimization empowered structure search and first-principles calculations within a wide pressure range of 200–400 GPa, covering the pressure range of Earth's core. This compound features layered  $\text{Xe}_6\text{C}_2\text{O}_4$  sublattices, showing distinct covalent Xe-C bonds, supported by the calculated electron localization function. The presence of the covalent bonds is further corroborated by the large value of the integrated crystal orbital Hamilton population ( $-4.02$  eV/pair) and the large negative Laplacian ( $-4.65$  e/Å<sup>5</sup>). This leads to an unusual  $sp^3$ -like hybridization in carbon, involving two oxygen atoms, one carbon atom, and one xenon atom. Additionally, two-phase method molecular dynamics simulations suggest that the compound exhibits liquid-state behavior at 200 GPa and 5000 K above the geotherm of the Earth's core. This shows a potential role for the compound in the liquid phase as a reservoir for the “missing Xe” phenomenon. Our findings not only enhance the understanding of bonding behavior in noble gas compounds, but also suggest the potential presence of  $\text{Xe}_3\text{CO}_2$  in various astronomical objects.

DOI: [10.1103/PhysRevB.110.054108](https://doi.org/10.1103/PhysRevB.110.054108)

### I. INTRODUCTION

Over the past few decades, research into noble gas (NG) elements has expanded [1–5], particularly under extreme conditions that induce novel chemical valence states [6,7]. Extensive investigations [8–13] have been conducted to explore noble gas compounds under high pressure and high temperature (HPHT). Advances in computational physics have revealed how pressure affects xenon, and some theoretical studies have unveiled the influence of pressure on xenon, resulting in the emergence of diverse oxidation states. These results have shown that xenon can form compounds with ionic [14–16] and covalent bonds [17,18], and have also highlighted the fascinating emergence of electrified [19]. These findings have stimulated further research into the discovery of NG compounds under high-pressure conditions.

The properties of high-pressure NG compounds are increasingly recognized as pertinent to planetary processes and mysteries [9,11,20,21]. For instance, to explore the elusive “missing Xe” (the relative depletion of Earth's atmospheric Xe compared with Ar and Kr—the geochemical missing Xe problem [22,23])—suggests that significant amounts of Earth's primordial Xe could be sequestered at depth, inside the core [9]), some previous research indicates that the Xe element can be trapped in  $\text{SiO}_2$  samples [24] or supercells in Fe [25] by experiment. Recently, a different understanding from the point of chemical stability shows that if Xe

were captured, it would have chemically stable compounds, and stable Xe-Fe/Ni compounds are proposed to serve as a reservoir for the Xe element in the Earth's core theoretically [9]. Subsequently, another stable compound formed by Xe and suitable minerals  $\text{FeO}_2$  has been predicted to provide a mineral repository for the Xe element. Furthermore, in addition to the high-pressure compounds formed by these inert elements with common minerals, certain compounds composed of volatile substances are also deemed significant within the Earth's interior [26–28]. In our recent work, we proposed the existence of  $\text{H}_2\text{O-N}_2$  compounds formed under extreme conditions in the Earth's mantle through subduction extending into the deep mantle [28]. This finding offers insights into the “missing nitrogen” enigma. One can raise a question: Are there volatile compounds in the Earth's interior that can react with Xe at the extreme conditions of the Earth's interior? Given the abundance and significance of  $\text{CO}_2$ , similar to  $\text{H}_2\text{O}$  and  $\text{N}_2$ , within the Earth, exploring  $\text{CO}_2$ -bearing compounds in the deep Earth emerges as a promising area of research, potentially unveiling new insights into Earth's composition and processes.

With computational physics and density functional theory rapidly developing, newly predicted discoveries of compounds, different from the traditional minerals, have provided vital insights into the mechanisms and minerals in the planetary interior through the combination of structural prediction and *ab initio* simulations. Here, we choose Xe and  $\text{CO}_2$ , fundamental molecules that are abundant in the Earth's environment [32,33], expecting the reaction at the extreme condition of Earth's interior. Although the high-pressure phases of  $\text{CO}_2$  and its compounds have been identified at

\*Contact author: kevin.m.yang@polyu.edu.hk

†Contact author: tzhou@eitech.edu.cn

pressures reaching hundreds of gigapascals [29,34,35], studies on the high-pressure behaviors of the Xe-CO<sub>2</sub> system and their implications for Earth's mysteries remain scarce. In this paper, we investigate the behavior of the Xe-CO<sub>2</sub> system under high pressure. The binary convex hull analysis reveals the existence of a compound, Xe<sub>3</sub>CO<sub>2</sub>, with the *C2/m* space group. This compound exhibits a unique bonding arrangement: Xenon forms ionic bonds with oxygen and covalent bonds with carbon, including rare covalent Xe-C bonds. These bonds, together with the conventional covalent C-O and C-C bonds, result in a *sp*<sup>3</sup>-like configuration centered on C. Furthermore, two-phase method molecular dynamics simulations demonstrate that Xe<sub>3</sub>CO<sub>2</sub> exhibits liquid-state properties at high temperatures, akin to those in the Earth's core, offering insights into the missing Xe puzzle in the deep Earth.

## II. METHODS

We conducted extensive searches to explore the structural properties of various compositions in the Xe-CO<sub>2</sub> system at high pressures of 200, 300, and 400 GPa. We used the CALYPSO algorithm to identify the stable and metastable crystalline structures [36–39], which is highly effective for structural predictions [40–43]. To further investigate the structural and electronic properties of the stable Xe-CO<sub>2</sub> compounds, we employed the density functional theory (DFT)-based Vienna *ab initio* simulation package [44,45]. For the exchange-correlation potential, we adopted the generalized gradient approximation (GGA) [45] in the form of the Perdew-Burke-Ernzerhof (PBE) [46] functional. We utilized the projector augmented-wave (PAW) method for electron-ion interactions, in which the valence electrons of *5s*<sup>2</sup>*5p*<sup>6</sup>, *2s*<sup>2</sup>*2p*<sup>2</sup>, and *2s*<sup>2</sup>*2p*<sup>4</sup> for Xe, C, and O were considered, respectively. The first Brillouin zone was sampled by using Monkhorst-Pack *k* points with a grid density of 0.2 Å<sup>-1</sup> to achieve convergence in total energy (better than 1 meV per atom). The plane-wave basis set was expanded up to a cutoff energy of 800 eV. We used the Methfessel-Paxton method for partial occupancy (ISMEAR = 1) with a small SIGMA value of 0.05 for the DFT calculation. These methods and parameters are standard for such kinds of calculations and have been validated as accurate in numerous publications. We performed phonon calculations with a grid density of 0.2 Å<sup>-1</sup> using the 1 × 2 × 2 supercell method implemented in the PHONOPY code [47]. To study the matter states of Xe<sub>3</sub>CO<sub>2</sub>, a two-phase model of a coexisting solid and liquid with a ratio of approximately 1:1 is built. In this study, we employ 2 × 2 × 4 supercells comprising 384 atoms for our calculations, although larger supercells could be utilized to enhance accuracy [48], and then relaxed for 1000 steps at the desired pressure and temperature conditions in the *NPT* ensemble. The relaxed cell is then used to perform *NVT* simulations at high temperatures far exceeding the melting temperatures with the atoms of half the cell fixed and the force applied to these atoms set to be 0. Therefore, we obtain coexisting phases of the solid and liquid phases. Simulations on the two-phase cell were performed at the desired pressure and temperature conditions (*NPT*) with only the  $\Gamma$  point for the Brillouin zone sampling and the time interval is 1 fs. In addition to this method, we also do dynamical simulations, which were performed in the

canonical (*NVT*) ensemble applying the Nosé-Hoover thermostat combining with a supercell method (192 atoms) with only the  $\Gamma$  point for the Brillouin zone sampling to determine the dynamical properties at high temperatures. Each simulation consists of 14 000 time steps with a time step of 1 fs. Similar to the common methods in previous research, our structure search calculations are performed at 0 K. To visualize the crystal structures and electron localization function (ELF), we utilize the VESTA software [49].

## III. RESULTS

In our investigation of the Xe-CO<sub>2</sub> system, we have conducted multiple simulations to predict the stable structure with varied compositions [Xe<sub>*x*</sub>(CO<sub>2</sub>)<sub>*y*</sub>, *x* = 1–4, *y* = 1–4], with maximum atoms in a cell up to 44 atoms at the pressure of 200, 300, and 400 GPa. For each prediction, we sampled over 2000 structures and selected at least ten potential structures as candidates for further accurate optimization. To assess the thermodynamic stability of the predicted structures, we construct a binary convex hull using a formation enthalpy (*H*) formula  $\Delta H = H[\text{Xe}_x(\text{CO}_2)_y] - xH(\text{Xe}) - yH(\text{CO}_2)/(x + y)$ . One specific compound of interest is the Xe<sub>3</sub>CO<sub>2</sub> compound, which has a 3:1 ratio of Xe to CO<sub>2</sub>. It is found to lie on the convex hull between 200 and 300 GPa, indicating its thermodynamic stability under high pressure [solid symbol in Fig. 1(a)], while other stoichiometries lie above the convex hull, exhibiting instability [open symbol in Fig. 1(a)]. To elaborate the physical mechanism on the reaction of 3Xe + CO<sub>2</sub> → Xe<sub>3</sub>CO<sub>2</sub>, we calculate the  $\Delta(PV)$ ,  $\Delta U$ , and  $\Delta H$  in the reaction. Figure 1(b) shows that  $\Delta(PV)$  is negative, and the  $\Delta U$  term remains positive with a more substantial reduction. At 247 GPa, according to the formula ( $H = U + PV$ ), the  $\Delta U$  enable the  $\Delta H$  to have a negative value, where Xe<sub>3</sub>CO<sub>2</sub> start to stabilize.

*C2/m*-Xe<sub>3</sub>CO<sub>2</sub> consists of layered Xe<sub>6</sub>C<sub>2</sub>O<sub>4</sub> units, as depicted in Fig. 2(a). Within each unit, CO<sub>2</sub> polymerizes into C<sub>2</sub>O<sub>4</sub>, which is embedded in a ring of six Xe atoms. The C atom in C<sub>2</sub>O<sub>4</sub> forms bonds with two O atoms, resulting in C-O distances of 1.27 Å, similar to the experimentally observed C-O bond length of 1.27 Å in oxalate [50]. These CO<sub>2</sub> units connect with each other through the C-C bond, which is measured at 1.36 Å. Interestingly, the C-O bonds at both ends of the C-C bond face the opposite direction. Regarding the Xe-Xe distances, they range from 2.66 to 3.01 Å, which is significantly larger than the covalent radius 1.4 Å of Xe [51], excluding any Xe-Xe bonding possibility. The interlayer distance is determined by the shortest Xe-O bond length. The Xe1 atoms (orange) form bonds with their nearest neighboring O atoms with a bond length of 2.12 Å, as shown in Fig. 2(a). Notably, the nearest Xe-C distances are 2.04 Å, smaller than 2.16 Å, the sum of covalent radii of the Xe and C atoms [51], indicating a potentially covalent Xe-C bond. Further analysis on this bonding will be discussed later. From the top view in Fig. 2(b), we can see that Xe<sub>6</sub>C<sub>2</sub>O<sub>4</sub> units are stacked to form a confined space. Due to the interaction between the Xe1 and O, the interior space is slightly distorted, adopting an S-shaped configuration. This arrangement enhances structural stability by adopting a denser structure.

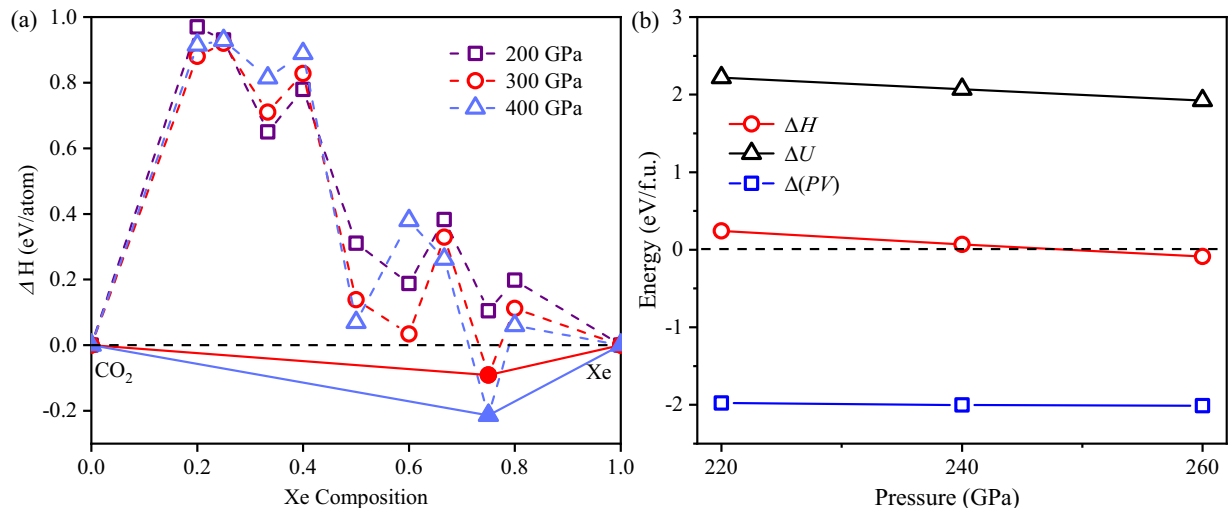


FIG. 1. (a) Calculated thermodynamic stability of Xe<sub>3</sub>CO<sub>2</sub> compounds, where the stable structures of hcp-Xe at 200–400 GPa,  $\bar{I}42d$ -CO<sub>2</sub> at 200–285 GPa, and  $P4_2/nmc$ -CO<sub>2</sub> at 285–400 GPa are adopted in Refs. [29,30]. The open and solid symbols represent the unstable and stable stoichiometries. (b) Pressure-dependent variation of enthalpy ( $\Delta H$ ), pressure-volume ( $\Delta PV$ ) term, and internal energy ( $\Delta U$ ) for Xe<sub>3</sub>CO<sub>2</sub>. The relevant structure information is given in the structural information of Table S1 in the Supplemental Material (SM) [31].

To analyze bonding characteristics, the ELF is employed as a quantitative measure. The value of ELF ranges between 0 and 1, with 0.5 representing the state observed in a homogeneous electron gas. The localization of electrons at the respective bond junctions substantiates the classical covalent bonding patterns of C-O and C-C, as depicted in Fig. S1 in SM [31]. Notably, further analysis reveals a localized charge distribution between Xe and C, with ELF values between 0.6 and 0.8 [Fig. 3(a)]. A value exceeding 0.5 is typically indicative of the tendencies for electron pairing, signifying the presence of chemical bonds, lone pairs of electrons, or electrodes. To further characterize the nature of the Xe-C bond, calculations of the crystal orbital Hamilton population (COHP) [52] are performed. At 300 GPa, we observe the bonding state of Xe and C below the Fermi level ( $E_f$ ), as

illustrated in Fig. 3(b). This results in the integrated crystal orbital Hamilton population (ICOHP) value of  $-4.02$  eV/pair for the Xe-C bond length, comparable to  $-4.06$  eV/pair of the covalent bond of H-H in HfH<sub>9</sub> [53] but significantly lower than  $-0.9$  eV/pair of Na-Na in electride Na<sub>2</sub>He [1].

This suggests the great difference in the bonding characteristic with electrode compounds. Furthermore, each C atom possesses four valence electrons, with two electrons covalently bonded to the O atom and one electron covalently bonded to another C atom. The remaining electron satisfies the octet rule by forming a chemical bond, eliminating the existence of lone pairs of electrons. The quantum theory of atoms in molecules (QTAIM) has been successfully used to identify covalent bonds in various systems [18,54]. Therefore, we also employed QTAIM to reveal the bonding characteristic in Xe<sub>3</sub>CO<sub>2</sub>, in which the Laplacian of the electron density is examined for the Xe-C bond. The calculated value is

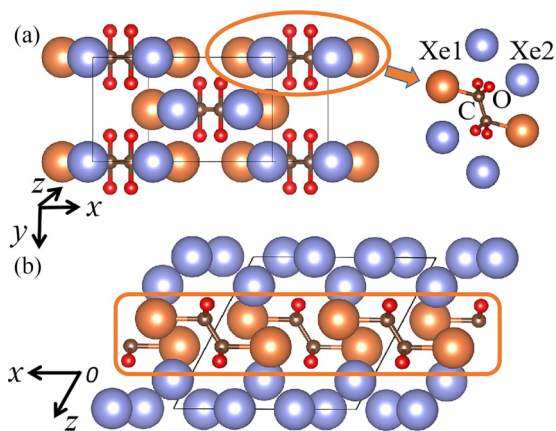


FIG. 2. (a) Side view and (b) top view of the  $C2/m$ -Xe<sub>3</sub>CO<sub>2</sub> phase at 300 GPa. An orange circle highlights the Xe<sub>6</sub>C<sub>2</sub>O<sub>4</sub> unit, and an orange rectangle indicates the region of Xe-C covalent bond formation. The Xe atoms bonded and unbonded with C atoms are labeled as Xe1 (orange) and Xe2 (blue), respectively.

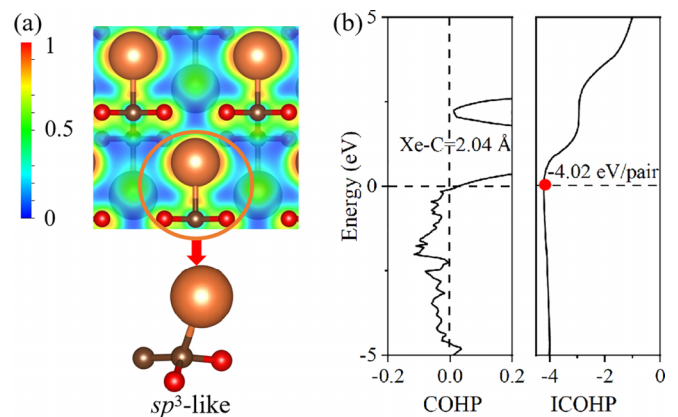


FIG. 3. (a) Visualized ELF plots for the covalent Xe-C bond at 300 GPa, where the C atom with fourfold bonding ( $sp^3$ -like hybridization) is highlighted. (b) Calculated COHP and ICOHP of the Xe-C pair, with a bond length of  $2.04$  Å.

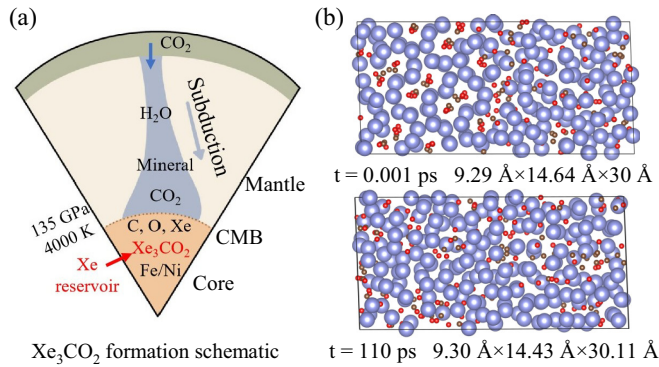


FIG. 4. (a) Schematic illustrating  $\text{Xe}_3\text{CO}_2$  formation through the Earth’s mantle subduction or as a core volatile. (b) MD simulation of their coexistence at 200 GPa and 5000 K.

$-4.65 e/\text{\AA}^5$ , which is comparable to the value of  $-5.09 e/\text{\AA}^5$  observed for a typical covalent H-S bond in  $\text{H}_3\text{S}$  [54]. This strongly suggests the presence of a covalent bond between Xe and C. Based on these observations, we propose that the C atom undergoes  $sp^3$  hybridization with two O atoms, one C atom, and one Xe atom through covalent interactions, as shown in Fig. 3. These results indicate that diverse interactions among Xe, C, and O atoms mainly occur in the orange square, as marked in Fig. 2(b), and Xe2 atoms play a great role in building the structural framework.

To evaluate the structural stability, we calculate the phonon dispersion using the finite displacement in the supercells. The absence of any negative vibrational frequencies in the phonon dispersion spectrum indicates the dynamic stability of the system, as depicted in Fig. S2 in SM [31]. Further analysis reveals that the vibrational modes can be categorized into two distinct groups. The first group, with frequencies ranging from 0 to 25 THz, primarily results from the interactions among all atoms, especially between Xe and C atoms. Conversely, the second group, with frequencies from 25 to 50 THz, is associated exclusively with the vibrations of C-O bonds. The electronic band structures and density of states (Fig. S3 in SM [31]) reveal a metallic character of  $\text{Xe}_3\text{CO}_2$  due to the presence of Xe-derived states near the  $E_f$ . Below the  $E_f$ , we can see the hybridization of Xe and C atoms, corresponding to the bonding state observed in the COHP analysis [Fig. 3(b)].

Previous studies have highlighted the potential for a Xe reservoir in the HPHT conditions of deep Earth [9] and the significant transport of  $\text{CO}_2$  into the deep Earth through subduction processes [55]. Therefore, it is worthwhile to explore the possibility of the existence of  $\text{Xe}_3\text{CO}_2$  in the deep Earth and its connection with planetary phenomena. We first obtained its HPHT phase diagram through the quasiharmonic approximation methods, which shows a wide pressure range of the thermodynamical stability as seen in Fig. S4 of SM [31]. Then we used a two-phase method to perform a molecular dynamics simulation to examine the matter state of  $\text{Xe}_3\text{CO}_2$  within its stable range. Figure 4(b) presents the coexistence of  $\text{Xe}_3\text{CO}_2$  (upper panel) at 200 GPa and 5000 K above the geotherm of Earth’s core. After 110 ps, all atoms diffuse their equilibrium position and the simulation melts, as shown in the

lower panel of Fig. 4(b). It signifies a liquid phase. Further simulations at 260 GPa and 5500 K above the geotherm of Earth’s core also confirm the presence of a liquid phase, as shown in Fig. S5 in SM [31]. These results indicate that the liquid  $\text{Xe}_3\text{CO}_2$ ’s stability extends to extreme conditions akin to Earth’s core. It is interesting that we also used the single-phase method (*NVT*) to consider the matter states of  $\text{Xe}_3\text{CO}_2$ . Figures S6 and S7 in SM [31] present the calculated results at 220 GPa and 5000 K, and 283 GPa and 5700 K. While the hydrostatic pressure is considered here, the nonhydrostatic components of the stress matrix should be carefully addressed in low-symmetry systems. It clearly shows that all atoms exhibit vibrations around their equilibrium positions, which indicates a totally different solid phase. Since we consider the solid-liquid interface as the nucleation point in the half-solid and half-liquid structure, it can avoid the superheating usually happening in the single phase. On the other hand, the inhomogeneous nucleation process in the two-phase method, different from the homogeneous nucleation process in the single-phase method, is close to the experimental condition [56]. To some extent, we can infer relatively highly accurate results through the two-phase method, but it should be noted that both methods are widely used in the research. Additionally, we provide insights into the formation of  $\text{Xe}_3\text{CO}_2$  through Earth’s internal processes as shown in Fig. 4(a). The deep Earth’s subduction processes, involving significant  $\text{CO}_2$ , may facilitate latent xenon to form  $\text{Xe}_3\text{CO}_2$ , hinting at a xenon reservoir. Moreover, the plausible major light elements such as C and O may offer an opportunity for  $\text{Xe}_3\text{CO}_2$  formation through these elements under extreme conditions.

#### IV. CONCLUSIONS

In conclusion, our research identifies a different, stable compound,  $\text{Xe}_3\text{CO}_2$ , under high pressure, through a structural search with DFT calculations. The pressure-induced variation of the internal energy stabilizes the structure at 247 GPa. Bonding pattern analysis reveals an exotic Xe-C covalent bond, as evidenced by various methods (such as ELF, ICOHP, and QTAIM). Consequently, a  $sp^3$ -like configuration of carbon is characterized by a traditional covalent C-O bond and a covalent C-C bond, alongside the distinctive covalent Xe-C bond. Further calculations demonstrate that the predicted compounds transition to a liquid phase at HPHT, mirroring those of Earth’s interior. Such findings imply that the  $\text{Xe}_3\text{CO}_2$  compound could potentially serve as an Xe reservoir. Our work not only advances our understanding of xenon chemistry but also contributes valuable insights for Earth’s interior models and for the “missing Xe” mystery.

#### ACKNOWLEDGMENTS

M.Y. acknowledges the funding support from The Hong Kong Polytechnic University (Projects No. P0049524, No. P0048122, and No. P0034827) and the Research Grants Council, Hong Kong (Projects No. 25301523 and 15307124). The computing for this research was supported by High Performance Computing Platform at the Eastern Institute of Technology, Ningbo.

- [1] X. Dong, A. R. Oganov, A. F. Goncharov, E. Stavrou, S. Lobanov, G. Saleh, G.-R. Qian, Q. Zhu, C. Gatti, V. L. Deringer *et al.*, A stable compound of helium and sodium at high pressure, *Nat. Chem.* **9**, 440 (2017).
- [2] Y. Li, X. Feng, H. Liu, J. Hao, S. A. Redfern, W. Lei, D. Liu, and Y. Ma, Route to high-energy density polymeric nitrogen *t*-N via He-N compounds, *Nat. Commun.* **9**, 722 (2018).
- [3] H. Liu, Y. Yao, and D. D. Klug, Stable structures of He and H<sub>2</sub>O at high pressure, *Phys. Rev. B* **91**, 014102 (2015).
- [4] J. Hou, X. Dong, A. R. Oganov, X.-J. Weng, C.-M. Hao, G. Yang, H.-T. Wang, X.-F. Zhou, and Y. Tian, Helium-bearing superconductor at high pressure, *Phys. Rev. B* **106**, L220501 (2022).
- [5] Z. Liu, J. Botana, A. Hermann, S. Valdez, E. Zurek, D. Yan, H.-q. Lin, and M.-s. Miao, Reactivity of He with ionic compounds under high pressure, *Nat. Commun.* **9**, 951 (2018).
- [6] M. Miao, Noble gases in solid compounds show a rich display of chemistry with enough pressure, *Front. Chem.* **8**, 570492 (2020).
- [7] M. Xu, Y. Li, and Y. Ma, Materials by design at high pressures, *Chem. Sci.* **13**, 329 (2022).
- [8] N. Bartlett, Xenon hexafluoroplatinate (V) Xe<sup>+</sup>[PtF<sub>6</sub>]<sup>-</sup>, *Proc. Chem. Soc.* **6**, 218 (1962).
- [9] L. Zhu, H. Liu, C. J. Pickard, G. Zou, and Y. Ma, Reactions of xenon with iron and nickel are predicted in the Earth's inner core, *Nat. Chem.* **6**, 644 (2014).
- [10] J. Zhang, H. Liu, Y. Ma, and C. Chen, Direct H-He chemical association in superionic FeO<sub>2</sub>H<sub>2</sub> He at deep-Earth conditions, *Natl. Sci. Rev.* **9**, nwab168 (2022).
- [11] J. Shi, W. Cui, J. Hao, M. Xu, X. Wang, and Y. Li, Formation of ammonia-helium compounds at high pressure, *Nat. Commun.* **11**, 3164 (2020).
- [12] S. Ding, P. Zhang, K. Yang, C. Liu, J. Hao, W. Cui, J. Shi, and Y. Li, Formation of solid SiO<sub>2</sub>He compound at high pressure and high temperature, *Phys. Rev. B* **106**, 024102 (2022).
- [13] C. Liu, J. Wang, X. Deng, X. Wang, C. J. Pickard, R. Helled, Z. Wu, H.-T. Wang, D. Xing, and J. Sun, Partially diffusive helium-silica compound under high pressure, *Chin. Phys. Lett.* **39**, 076101 (2022).
- [14] Z. Liu, J. Botana, M. Miao, and D. Yan, Unexpected Xe anions in XeLi<sub>*n*</sub> intermetallic compounds, *Europhys. Lett.* **117**, 26002 (2017).
- [15] N. Zarifi, H. Liu, J. S. Tse, and E. Zurek, Crystal structures and electronic properties of Xe-Cl compounds at high pressure, *J. Phys. Chem. C* **122**, 2941 (2018).
- [16] M. Zou, K. Yang, P. Zhang, W. Cui, J. Hao, J. Shi, and Y. Li, Existence of solid Na-Xe compounds at the extreme conditions of Earth's interior, *Phys. Rev. Res.* **5**, 043107 (2023).
- [17] F. Peng, J. Botana, Y. Wang, Y. Ma, and M. Miao, Unexpected trend in stability of Xe-F compounds under pressure driven by Xe-Xe covalent bonds, *J. Phys. Chem. Lett.* **7**, 4562 (2016).
- [18] F. Peng, Y. Wang, H. Wang, Y. Zhang, and Y. Ma, Stable xenon nitride at high pressures, *Phys. Rev. B* **92**, 094104 (2015).
- [19] M. s. Miao, X. l. Wang, J. Brgoch, F. Spera, M. G. Jackson, G. Kresse, and H.-q. Lin, Anionic chemistry of noble gases: formation of Mg-NG (NG=Xe, Kr, Ar) compounds under pressure, *J. Am. Chem. Soc.* **137**, 14122 (2015).
- [20] C. Liu, H. Gao, Y. Wang, R. J. Needs, C. J. Pickard, J. Sun, H.-T. Wang, and D. Xing, Multiple superionic states in helium-water compounds, *Nat. Phys.* **15**, 1065 (2019).
- [21] J. Zhang, J. Lv, H. Li, X. Feng, C. Lu, S. A. T. Redfern, H. Liu, C. Chen, and Y. Ma, Rare helium-bearing compound FeO<sub>2</sub> He stabilized at deep-earth conditions, *Phys. Rev. Lett.* **121**, 255703 (2018).
- [22] E. Anders and T. Owen, Mars and Earth: Origin and abundance of volatiles, *Science* **198**, 453 (1977).
- [23] I. Tolstikhin and R. O'Nions, The Earth's missing xenon: A combination of early degassing and of rare gas loss from the atmosphere, *Chem. Geol.* **115**, 1 (1994).
- [24] C. Sanloup, B. C. Schmidt, E. M. C. Perez, A. Jambon, E. Gregoryanz, and M. Mezouar, Retention of xenon in quartz and Earth's missing xenon, *Science* **310**, 1174 (2005).
- [25] K. K. Lee and G. Steinle-Neumann, High-pressure alloying of iron and xenon: 'Missing' Xe in the Earth's core? *J. Geophys. Res.: Solid Earth* **111**, B02202 (2006).
- [26] S. Liu, P. Gao, A. Hermann, G. Yang, J. Lü, Y. Ma, H.-K. Mao, and Y. Wang, Stabilization of S<sub>3</sub>O<sub>4</sub> at high pressure: Implications for the sulfur-excess paradox, *Sci. Bull.* **67**, 971 (2022).
- [27] S. Liu, W. Lu, X. Zhang, J. Song, J. Lü, X. Liu, Y. Wang, C. Chen, and Y. Ma, A viable mechanism to form boron-bearing diamonds in deep Earth, *Sci. Bull.* **68**, 1456 (2023).
- [28] K. Yang, J. Shi, W. Cui, J. Hao, and Y. Li, Prediction of a reservoir of N-rich high-energy density material at the Earth's mantle, *Phys. Chem. Chem. Phys.* **25**, 20281 (2023).
- [29] C. Lu, M. Miao, and Y. Ma, Structural evolution of carbon dioxide under high pressure, *J. Am. Chem. Soc.* **135**, 14167 (2013).
- [30] E. Kim, M. Nicol, H. Cynn, and C.-S. Yoo, Martensitic fcc-to-hcp transformations in solid xenon under pressure: A first-principles study, *Phys. Rev. Lett.* **96**, 035504 (2006).
- [31] See Supplemental Material at <http://link.aps.org/supplemental/10.1103/PhysRevB.110.054108> for the expanded discussion about the Xe<sub>3</sub>CO<sub>2</sub> details including the electron localization function, mean-squared displacement, structural parameters, band structures, phonon dispersion, and atomic trajectories.
- [32] S. Mukhopadhyay and R. Parai, Noble gases: A record of Earth's evolution and mantle dynamics, *Annu. Rev. Earth Planet. Sci.* **47**, 389 (2019).
- [33] T. Plank and C. E. Manning, Subducting carbon, *Nature (London)* **574**, 343 (2019).
- [34] D. Li, Y. Liu, F. Tian, S. Wei, Z. Liu, D. Duan, B. Liu, and T. Cui, High-pressure structures of helium and carbon dioxide from first-principles calculations, *Solid State Commun.* **283**, 9 (2018).
- [35] B. Huang and G. Frapper, Pressure-induced polymerization of CO<sub>2</sub> in lithium-carbon dioxide phases, *J. Am. Chem. Soc.* **140**, 413 (2018).
- [36] Y. Wang, J. Lv, L. Zhu, and Y. Ma, Crystal structure prediction via particle-swarm optimization, *Phys. Rev. B* **82**, 094116 (2010).
- [37] Y. Wang, J. Lv, L. Zhu, and Y. Ma, CALYPSO: A method for crystal structure prediction, *Comput. Phys. Commun.* **183**, 2063 (2012).
- [38] B. Gao, P. Gao, S. Lu, J. Lv, Y. Wang, and Y. Ma, Interface structure prediction via CALYPSO method, *Sci. Bull.* **64**, 301 (2019).
- [39] X. Shao, J. Lv, P. Liu, S. Shao, P. Gao, H. Liu, Y. Wang, and Y. Ma, A symmetry-orientated divide-and-conquer method for crystal structure prediction, *J. Chem. Phys.* **156**, 014105 (2022).

- [40] H. Liu, I. I. Naumov, R. Hoffmann, N. Ashcroft, and R. J. Hemley, Potential high- $T_c$  superconducting lanthanum and yttrium hydrides at high pressure, *Proc. Natl. Acad. Sci. USA* **114**, 6990 (2017).
- [41] W. Cui, T. Bi, J. Shi, Y. Li, H. Liu, E. Zurek, and R. J. Hemley, Route to high- $T_c$  superconductivity via  $\text{CH}_4$ -intercalated  $\text{H}_3\text{S}$  hydride perovskites, *Phys. Rev. B* **101**, 134504 (2020).
- [42] Y. Li, J. Hao, H. Liu, Y. Li, and Y. Ma, The metallization and superconductivity of dense hydrogen sulfide, *J. Chem. Phys.* **140**, 174712 (2014).
- [43] F. Peng, Y. Sun, C. J. Pickard, R. J. Needs, Q. Wu, and Y. Ma, Hydrogen clathrate structures in rare earth hydrides at high pressures: Possible route to room-temperature superconductivity, *Phys. Rev. Lett.* **119**, 107001 (2017).
- [44] G. Kresse and J. Furthmüller, Efficient iterative schemes for *ab initio* total-energy calculations using a plane-wave basis set, *Phys. Rev. B* **54**, 11169 (1996).
- [45] J. P. Perdew, K. Burke, and M. Ernzerhof, Generalized gradient approximation made simple, *Phys. Rev. Lett.* **77**, 3865 (1996).
- [46] P. E. Blöchl, O. Jepsen, and O. K. Andersen, Improved tetrahedron method for Brillouin-zone integrations, *Phys. Rev. B* **49**, 16223 (1994).
- [47] A. Togo, F. Oba, and I. Tanaka, First-principles calculations of the ferroelastic transition between rutile-type and  $\text{CaCl}_2$ -type  $\text{SiO}_2$  at high pressures, *Phys. Rev. B* **78**, 134106 (2008).
- [48] J. Deng, H. Niu, J. Hu, M. Chen, and L. Stixrude, Melting of  $\text{MgSiO}_3$  determined by machine learning potentials, *Phys. Rev. B* **107**, 064103 (2023).
- [49] K. Momma and F. Izumi, VESTA3 for three-dimensional visualization of crystal, volumetric and morphology data, *J. Appl. Crystallogr.* **44**, 1272 (2011).
- [50] M. Marqués, M. I. McMahon, E. Gregoryanz, M. Hanfland, C. L. Guillaume, C. J. Pickard, G. J. Ackland, and R. J. Nelmes, Crystal structures of dense lithium: A metal-semiconductor-metal transition, *Phys. Rev. Lett.* **106**, 095502 (2011).
- [51] B. Cordero, V. Gómez, A. E. Platero-Prats, M. Revés, J. Echeverría, E. Cremades, F. Barragán, and S. Alvarez, Covalent radii revisited, *Dalton Trans.* **2008**, 2832 (2008).
- [52] R. Dronskowski and P. E. Blöchl, Crystal orbital Hamilton populations (COHP): energy-resolved visualization of chemical bonding in solids based on density-functional calculations, *J. Phys. Chem.* **97**, 8617 (1993).
- [53] K. Gao, W. Cui, J. Chen, Q. Wang, J. Hao, J. Shi, C. Liu, S. Botti, M. A. L. Marques, and Y. Li, Superconducting hydrogen tubes in hafnium hydrides at high pressure, *Phys. Rev. B* **104**, 214511 (2021).
- [54] B. Liu, W. Cui, J. Shi, L. Zhu, J. Chen, S. Lin, R. Su, J. Ma, K. Yang, M. Xu *et al.*, Effect of covalent bonding on the superconducting critical temperature of the HS-Se system, *Phys. Rev. B* **98**, 174101 (2018).
- [55] S. Tumiami, C. Tiraboschi, D. Sverjensky, T. Pettke, S. Recchia, P. Ulmer, F. Miozzi, and S. Poli, Silicate dissolution boosts the  $\text{CO}_2$  concentrations in subduction fluids, *Nat. Commun.* **8**, 616 (2017).
- [56] X. Wang, M. Yang, X. Gai, Y. Sun, B. Cao, J. Chen, M. Liang, F. Tian, and L. Li, A comprehensive investigation on the accuracy and efficiency of methods for melting temperature calculation using molecular dynamics simulations, *J. Mol. Liq.* **395**, 123924 (2024).